JJEE
Volume 7, Number 4, December 2021
Pages 344-359
Jordan Journal of Electrical Engineering
ISSN (Print): 2409-9600, ISSN (Online): 2409-9619

Performance Evaluation of DSTATCOM for 180 km 33 kV Feeder from Shinyanga to Bariadi in Tanzania

Godfrey Mhagama[1], Aviti T. Mushi[2*], Beda J. Kundy[3]

[1, 2, 3] Department of Electrical Engineering, University of Dar es Salaam, Dar es Salaam, Tanzania
E-mail: aviti.thadei@udsm.ac.tz; aviti.bahati@gmail.com
[1] Department of Computer Science and Engineering, University of Dar es Salaam, Dar es Salaam, Tanzania

Received: January 11, 2021 *Revised: May 31, 2021* *Accepted: June 09, 2021*

***Abstract*—** This article presents the performance evaluation of distribution static compensators (DSTATCOM) for the 180 km 33 kV line from Shinyanga to Bariadi in Tanzania. First, the voltage drop existing on the line is explained, and its negative consequences are mentioned. Secondly, the 180 km line is presented in the nominal π model. Then, DSTATCOM capacitive and inductive dynamic ranges of ± 1900 kVAr are calculated based on the system fault level. Using the energy storage of five cycles, a DC capacitor with a value of 0.19 mF is calculated. The DSTATCOM is designed using the voltage source converters (VSC) employing the neutral point clamped (NPC) topology. A proportional integral (PI) control algorithm was implemented to the DSTATCOM. Simulation of the modeled system of the feeder with DSTATCOM is carried out in MATLAB/Simulink environment for different loading conditions (light and heavy loading) to evaluate the steady-state performance. Simulation results reveal that for the light load of 0.45 MW, the receiving end voltage is 37.2 kV RMS and 31.5 kV RMS, before and after application of DSTATCOM, respectively. For the heavy load of 4.5 MW, the results are 28.45 kV RMS and 33.1 kV RMS, before and after application of DSTATCOM, respectively. The frequency-domain analysis reveals a gain margin of infinity implying stable system operation. The Nyquist plot shows no encirclement of the negative one point, further verifying the stability. It is concluded that the proposed DSTATCOM is capable of keeping both the voltage drop and rise of the line at acceptable levels for system stability of the Shinyanga-Bariadi feeder.

***Keywords*—** Distribution static compensators; Voltage source converters; Nominal π mode.

1. INTRODUCTION

Tanzanian medium voltage of 33 kV and 11 kV is used as the system voltage for primary distribution feeders. The design of these feeders is mainly radial topology. Due to the nature of dispersed and scattered load centers (towns) in Tanzania [1], the feeders have to run over long routes, such as the 180 km 33 kV Shinyanga–Bariadi line [2]. The feeder runs all this distance without any voltage control compensators; thus at the receiving end, it suffers a voltage drop of more than 7%. The result of this voltage drop is failing to start the large water pumping motors connected close to the end of the feeder, especially during peak load. Voltage improvement can be achieved using the volt-ampere reactive (VAR) compensation, series compensation and flexible alternating current transmission system (FACTS). However, these methods cannot handle dynamic voltage changes effectively. Therefore, fast reactive power compensation is necessary [3]. Distribution static synchronous compensator (DSTATCOM) can provide fast and continuous reactive power (Q) compensation to control the voltage of the feeder. However, off-the-shelf DSTATCOM cannot be used without the knowledge of the line parameters, control, power and other data of the feeder. Therefore, this paper proposes the use of the DSTATCOM for the 180 km 33 kV feeder for the Shinyanga–Bariadi line.

* Corresponding author
Article's DOI: 10.5455/jjee.204-1610344139

Power quality problems are inevitable due to the presence of nonlinear loads [4]. Nonlinear loads draw non-sinusoidal currents from the network and cause power quality problems [5]. The techniques to improve power quality are necessary due to the increasing trend of the use of nonlinear loads.

This paper is organized as follows: section 2 presents the Shinyanga–Bariadi feeder, covering the physical design, modeling and design of the DSTATCOM. Section 3 presents the field and simulation results together with the discussions. Section 4 presents the conclusions and future work in this direction.

2. MODELING THE SHINYANGA–BARIADI FEEDER

The mode of the 180 km 33 kV Shinyanga–Bariadi feeder, and the design of the DSTACOM are covered in the following subsections.

2.1. Description of the Feeder

Shinyanga–Bariadi radial feeder is captured in Fig. 1. It has a circuit breaker (CB) at the sending end at Shinyanga 220/33 kV substation. The line feeds Meatu, Malampaka, Maswa and Bariadi. Metering units and protection switchgear are installed at the sending end. These protection units include relays and the mentioned CB. Along the line, the spur lines are protected by dropout fuses. Switching is undertaken at Shinyanga. In case the dropout fuses fail to isolate a fault, the CB kicks in to isolate the feeder.

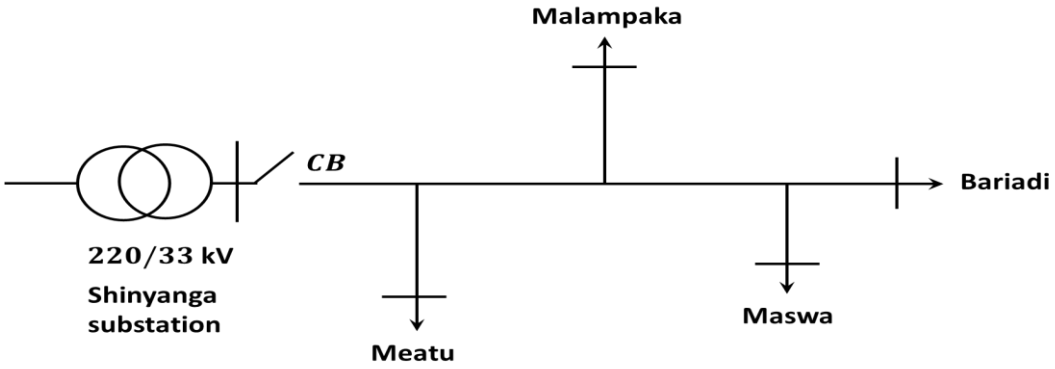

Fig. 1. Shinyanga–Bariadi radial feeder.

2.1.1. Design of the Feeder

Shinyanga–Bariadi radial feeder is constructed of wooden poles, aluminium conductor steel reinforced (ACSR) of 100 mm^2, porcelain insulators and other materials. The conductors are spaced at 1.2 m. This gives a geometric mean distance (GMD) of 1.5119 m. The feeder's recorded power for six months starting from December 2015 to May 2016 is shown in Table 1. The average of these maximum powers allows selecting the ACSR conductors based on the code given in Table 2.

Table 1. Highest recorded power on the Shinyanga–Bariadi feeder [6].

Power	Dec. 2015	Jan. 2016	Feb. 2016	Mar. 2016	Apr. 2016	May 2016
P [MW]	3.1	4.5	3.0	3.0	2.9	3.8
Q [MVAr]	2.0	2.2	2.2	2.2	3.8	2.6

Nominal powers (P_N and Q_N), nominal power factor angle (ϕ_N) and the feeder 33 kV taken as the nominal voltage (V_N) give together the feeder's nominal ampacity (I_N).

$$S_N = P_N + jQ_N;\ P_N = \frac{1}{N}\sum_{i=1}^{N} P_i;\ Q_N = \frac{1}{N}\sum_{i=1}^{N} Q_i;\ cos\phi_N = \frac{|P_N|}{|S_N|};\ I_N = \frac{\boldsymbol{P_N}}{\sqrt{3}V_N \cos\phi_N} \quad (1)$$

The nominal apparent power is represented by S_N. This is a very simple view, as load flow studies use the node voltages, currents, and admittance in power computations.

Table 2. ACSR specifications [7].

Conductor code	A_C [mm²]	A_{CI} [mm²]	R [Ω/km]	R_{AC} [Ω/km]	X [Ω/km]	Ampacity [A]
Dog	100	118.5	0.273	0.330	0.276	334
Leopard	125	138.78	0.2211	0.2212	0.2491	430
Dingo	150	167.485	0.1848	0.1848	0.2418	450
Hawk	242	280.903	0.1194	0.1198	0.2227	659
Bison	432	485	0.0757	0.0767	0.2092	855

According to IEC 60287-1-1 [7] and Riba [8], the values in per meter of R and R_{AC} are computed by Eqs. (2) and (3). The variables are: ρ_{20}- the resistivity at temperature ($T = 20\ ^{\circ}$C), α_{20} - the temperature coefficient at 20 °C, and A_{CI} - the cross-section of the ACSR conductor.

$$R = \frac{\rho_{20}}{A_{CI}}(1 + \alpha_{20}[T - T_{20}]) \quad (2)$$

$$R_{AC} = R(1 + y_s) \quad (3)$$

The skin effect factor (y_s) is computed from Eq. (4). The factor (x_s) is a constant computed by Eq. (5), and configuration constant $K_s = 1$ for the solid round conductor.

$$y_s = \frac{x_s^4}{192 + 0.8x_s^4} \quad (4)$$

$$x_s^4 = \left(\frac{8\pi f K_s}{R \times 10^7}\right)^2 \quad (5)$$

The $x_s \leq 2.8$ is the limit to meaningful applicability of Eq. (4). For larger values, other methods of computing R_{AC} are suggested by Riba [8]. The line capacitance (C), and inductance (L) per km are calculated by:

$$C = \frac{2\pi\varepsilon_0}{ln\left(\frac{GMD}{r}\right)};\ L = \frac{\mu_0}{2\pi}\left(\ln\left[\frac{GMD}{r}\right]\right) \quad (6)$$

The permittivity of free space is $\varepsilon_0 = 8.854 \times 10^{-12}$ F/m; permeability of free space is $\mu_0 = 4\pi \times 10^{-7}$ H/m; r is the radius of the ACSR conductor. The feeder inductive reactance (X), admittance (Y) and characteristic impedance (Z_C) are calculated by:

$$X = jwL,\ Y = jwC,\ Z_C = \sqrt{\frac{L}{C}} \quad (7)$$

2.1.2. Modeling the Distribution Feeder

The 180 km feeder is modeled using the nominal π model since it is a medium transmission line [9] captured by Fig. 2. The sending end voltage and current are V_S and I_S, respectively; X_{th} is the Thevenin equivalent reactance of the sending end; the R, X, and $Y$are the feeder's DC resistance, reactance, and admittance, respectively; the receiving end voltage and current are V_R and I_R, respectively and $Z_L$is the load. The nominal π model of the line - depicted in Fig. 2 - is presented by A, B, C^f, and D line parameters in Eqs. (8) and (9) [10]. The

line parameter C^f has been purposely defined to avoid confusion with the other line constant that was discussed prior. Here, it is assumed that V_S^{th} is the terminal voltage of the sending end. The line impedance is Z.

$$\begin{bmatrix} V_S^{th} \\ I_S \end{bmatrix} = \begin{bmatrix} A & B \\ C & D \end{bmatrix} \begin{bmatrix} V_R \\ I_R \end{bmatrix}; A = D = 1 + \frac{YZ}{2}; B = Z; C^f = Y\left(1 + \frac{YZ}{4}\right) \quad (8)$$

$$V_S = X_{th} I_S + V_S^{th}; Z = R + jX; V_R = Z_L I_R \quad (9)$$

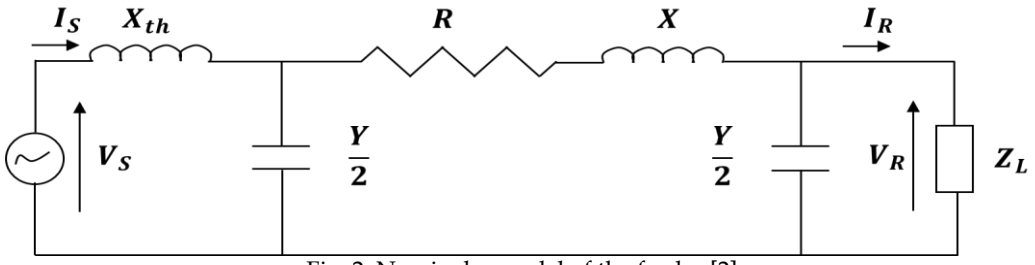

Fig. 2. Nominal π model of the feeder [2].

The design of this feeder considers a short circuit current ten times I_N (i.e., $I_{SC} = 10I_N$). Therefore, the short circuit apparent power is S_{SC} in Eq. (10). Then, the X_{th} is computed by Eq. (11). The receiving end powers – apparent, active, and reactive (i.e., $S_R = P_R + jQ_R$) are computed from Eqs. (12) and (13), and the voltage regulation (VR) is computed by Eq. (14).

$$S_{SC} = \sqrt{3}|V_N||I_{SC}| \quad (10)$$

$$X_{th} = \frac{|V_N|^2}{|S_{SC}|} \quad (11)$$

$$P_R = \frac{|V_S^{th}||V_R|}{|B|}\cos(\beta_B - \delta) - \frac{|A||V_R|^2}{|B|}\cos(\beta_B - \alpha_A) \quad (12)$$

$$Q_R = \frac{|V_S^{th}||V_R|}{|B|}\sin(\beta_B - \delta) - \frac{|A||V_R|^2}{|B|}\sin(\beta_B - \alpha_A) \quad (13)$$

$$VR = \frac{\frac{|V_S^{th}|}{|A|} - |V_R|}{|V_R|} \quad (14)$$

Other variables in Eqs. (12) and (13) are defined here and were computed by Eq. (8): β_B is the angle of the negative short circuit transfer impedance, δ is the sending end voltage angle and α_A is the angle of the open circuit voltage ratio.

2.2. Description of the DSTATCOM

The distribution static compensator is described in the section. First, the working principle is explained. Then, its design and sizing of the DC capacitor are presented, and lastly, the control part is elaborated.

2.2.1. Working Principle of DSTATCOM

Guerrero et al. [11] proposed DSTATCOM for voltage control of a feeder. This equipment works by injecting reactive power through shunt reactance (X_{DST}) to the feeder [12]. Fig. 3 shows a one-line equivalent diagram of DSTATCOM working to control the voltage of the point of common coupling (V_{PCC}), by injecting the DSTATCOM powers (P_{DST} and Q_{DST}) at the DSTATCOM voltage (V_{DST}) into the feeder at the point of common coupling (PCC).

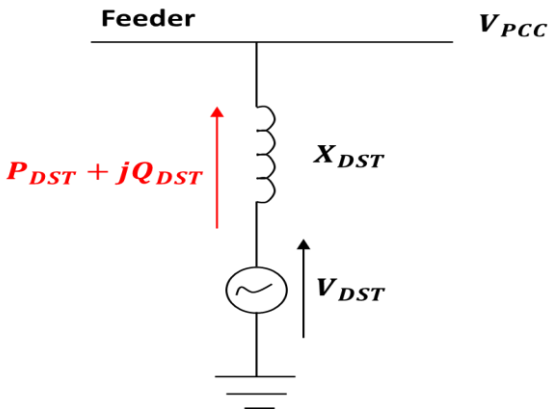

Fig. 3. One-line diagram of DSTATCOM.

This is how the DSTATCOM works:

- If $V_{DST} > V_{PCC}$, the DSTATCOM injects reactive power to the feeder;
- If $V_{DST} < V_{PCC}$, the DSTATCOM absorbs reactive power from the feeder; and
- If $V_{DST} = V_{PCC}$, the DSTATCOM is at equilibrium.

The power dynamics involved in the voltage control described above are encapsulated by the following expressions.

$$P_{DST} = \frac{|V_{PCC}||V_{DST}|}{X_{DST}} sin\delta_{DST} \quad (15)$$

$$Q_{DST} = \frac{|V_{PCC}|(|V_{PCC}| - |V_{DST}|cos\delta_{DST})}{X_{DST}} \quad (16)$$

The angle shift between V_{PCC} and V_{DST} is represented by δ_{DST}. The role of a control system in the DSTATCOM is to make V_{DST} in phase with V_{PCC} (i.e., $\delta_{DST} = 0$ radians) so that only the reactive power flows. Then, by Eq. (15), $P_{DST} = 0$ and Eq. (16) turns to Eq. (17).

$$Q_{DST} = \frac{|V_{PCC}|(|V_{PCC}| - |V_{DST}|)}{X_{DST}} \quad (17)$$

2.2.2. Design and Sizing the DSTATCOM

The DSTATCOM is designed using the three-level voltage source converter (VSC) with a neutral point clamped (NPC) topology. This topology is explained in detail by Mhagama [2] and Kerrouuche et al. [12]. This VSC NPC is a simpler design than the five-level flying capacitor VSC proposed by Roncero-Sanchez [13]. Sizing the DSTATCOM begins with selecting the short circuit power handling capability according to Eq. (10). Then, the allowable variation of the reactive power at the receiving end is selected to be $10\%S_{SC}$. Therefore, the dynamic range capability (Q_D) of the DSTATCOM will be computed by Eqs. (18) and (19), for which the percentage variation between the DSTATCOM output voltage and the feeder voltage is $\Delta V_{PCC}/V_{PCC}$ as in Eq. (20).

$$\pm\frac{1}{2}Q_D = Q_{DST} \quad (18)$$

$$Q_D = \left(0.1 - \frac{\Delta V_{PCC}}{V_{PCC}}\right) S_{SC} \quad (19)$$

$$\Delta V_{PCC} = V_{PCC} - V_{DST} \quad (20)$$

The energy storage capacitor (C_D) for the DSTATCOM DC link voltage U_D is designed to be able to store Q_D and discharge for five cycles (i.e., $t_D = 5\tau$) given by Eqs. (21) and (22) energy balance.

$$\frac{1}{2}C_D U_D^2 = Q_D t_D \quad (21)$$

$$C_D = 2\frac{Q_D}{U_D^2}t_D \quad (22)$$

Assuming ideal DSTATCOM switches and lossless coupling transformer, the DC storage capacitor voltage is related to the PCC voltage by Eq. (23). Note that $V_{PCC} = V_N = V_S$.

$$U_D = \frac{3\sqrt{2}}{\pi}V_N \quad (23)$$

2.2.3. Control of the DSTATCOM

The DSTATCOM is controlled by the industrially widely applicable proportional-integral controller (PI). Due to the nature of this controller, the synchronous reference frame ($d-q$ axis) is utilized. The frame rotates at the grid frequency so that the $d-q$ voltage (v_d, v_q) and currents (i_d, i_q, i_0) generated by the DSTATCOM is DC. The measured AC quantities are operated on by Park transformation (PkTF) to give the DC quantities, such as in Eq. (24).

$$\begin{bmatrix} i_d \\ i_q \\ i_0 \end{bmatrix} = \frac{2}{3}\begin{bmatrix} \sin\theta & \sin(\theta-\frac{2}{3}\pi) & \sin(\theta+\frac{2}{3}\pi) \\ \cos\theta & \cos(\theta-\frac{2}{3}\pi) & \cos(\theta+\frac{2}{3}\pi) \\ \frac{1}{2} & \frac{1}{2} & \frac{1}{2} \end{bmatrix}\begin{bmatrix} i_A \\ i_B \\ i_C \end{bmatrix} \quad (24)$$

The AC measured quantities are first passed through a low pass filter (LPF) to remove the measurement noises; the transfer function of the filter ($H_{LPF}(s)$) is given by Eq. (25). The feeder voltages (v_A, v_B, v_C or in short v_{ABC}), after passing through the LPF is used in the phase-locked loop (PLL) to generate the synchronous angle θ. These voltages are used to generate the voltage error from the reference $V_{ABC}^* = V_N = V_{PCC}$.

$$\mathrm{H(s)} = \frac{1}{1+s\tau_{LPF}} \quad (25)$$

$$\Delta v_{ABC} = V_{ABC}^* - v_{ABC} \quad (26)$$

This error is worked upon with the PI controller mentioned previously, and the output is the reference currents I_{ABC}^* presented in s domain by:

$$I_{ABC}^* = \left(K_p + \frac{K_i}{s}\right)\Delta v_{ABC} \quad (27)$$

The I_{ABC}^* is operated upon by an inverse PkTF to generate the reference currents in $d-q$ frame, I_{dq0}^*. This is used to generate error signal from measured, and low pass filtered line currents i_{ABC}. This current error is used to generate the six PWM pulses for the six legs of the VSC NPC. The control algorithm is shown in Fig. 4 excluding the grid and the VSC NPC parts.

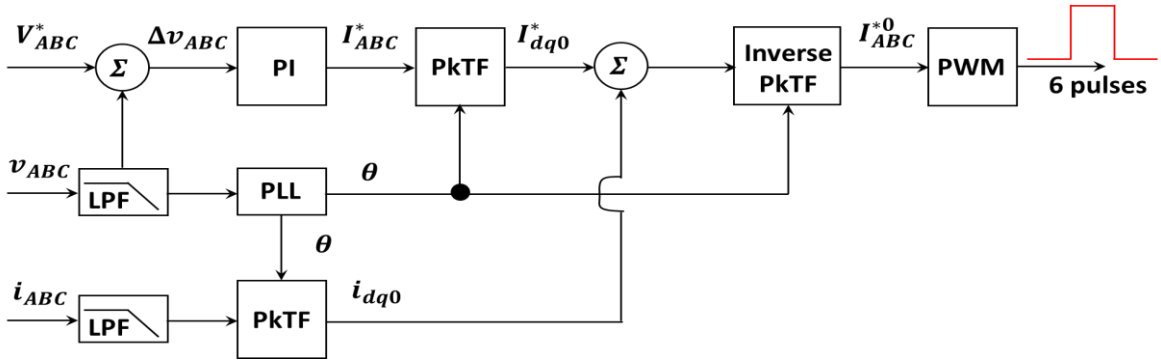

Fig. 4. The DSTATCOM control diagram.

The DSTATCOM implemented on the feeder's equivalent circuit is shown in Fig. 5. Note the DSTATCOM is represented as a voltage-controlled voltage source i.e., VCVS (U_D). This circuit renders itself to the transfer function given in Eq. (28). When the DSTATCOM is engaged in PI feedback loop, the closed-loop transfer function ($H_{CL}(s)$) will be as in Eq. (29).

$$H(s) = \frac{V_R(s)}{V_S(s)} \tag{28}$$

$$H_{CL}(s) = \frac{(K_p + K_i/s)H(s)}{1+(K_p+K_i/s)H(s)} \tag{29}$$

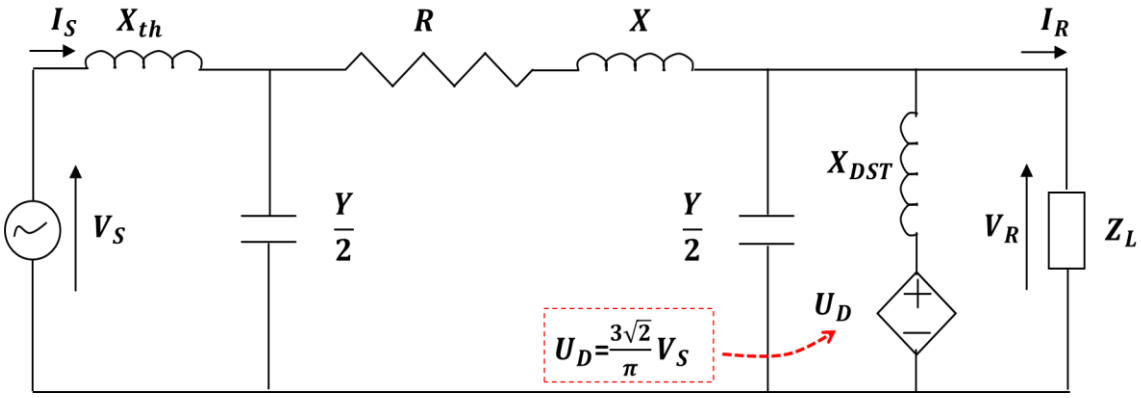

Fig. 5. Equivalent circuit diagram of the DSTATCOM installed at the feeder's receiving end.

2.3. Simulation of the Feeder and the DSTATCOM

The feeder model developed in section 2.1.2 and its DSTATCOM control developed in section 2.2.3 are implemented in MATLAB/Simulink. The sampling frequency is chosen as $f_S = 20$ kHz. Feeder frequency is set to $f = 50$ Hz giving a period of $\tau = 20$ ms. The chosen frequency is the power system frequency of Tanzania. The feeder is simulated for different scenarios – with and without DSTATCOM for light and heavy load.

3. RESULTS AND DISCUSSION

This section presents field data and the design results in addition to simulation results as was discussed in previous sections.

3.1. Field Data and Design of the Feeder and the DSTATCOM

The feeder's nominal voltage $V_N = 33$ kV is taken to be the PCC voltage, a short circuit current is selected as $I_{SC} = 10I_N = 910$ A, basing the $P_N = 3.8$ MW and $\cos(\theta_N) = 0.8$ from Table 2. The feeder's and DSTATCOM parameters are presented in Table 4.

Table 4. Feeder and DSTATCOM parameters.

Parameter	Value	Parameter	Value	Parameter	Value
A_{CI}	118.5 mm²	B	$81\angle 50.2^0$ Ω	$\lvert S_{SC}\rvert$	51.44 MVA
R	0.288 Ω/km	C^f	$0.00056\angle 90.42^0$ S	X_{th}	21.2 Ω
L	1.1 mH/km	D	$0.9825\angle 50.2^0$ Ω	$\frac{\Delta V_{PCC}}{V_{PCC}}$	2.5%
C	0.01 μF/km	Z_C	331.66 Ω	Q_{DST}	±1.90 MVAr
A	$0.9825\angle 0.85^0$	$\lvert I_{SC}\rvert$	910 A	C_D	0.190 mF

The PI controller was tuned in MATLAB using the sisotool giving controller gains shown in Table 5. The table also lists the period of the LPF. Parameters of Table 4 are used to compute the transfer function of the feeder and DSTATCOM as:

$$H(s) = \frac{1.35s^3+422.3s^2+1212.2s+0.07}{s^3+312.9s^2+897.9s} \quad (30)$$

Eq. (30) is used to elicit the frequency response of the feeder with the DSTATCOM by the Bode and Nyquist plots as shown by Figs. 6 and 7, respectively. From the Bode plot, the gain margin is infinity, and the phase margin is positive. From the Nyquist plot, there is no open-loop pole on the right half-plane.

Table 5. Controller and LPF gains.

Gain	Value
K_p	0.2 A/V
K_i	0.81 A/V/s
τ_{LPF}	30 ms

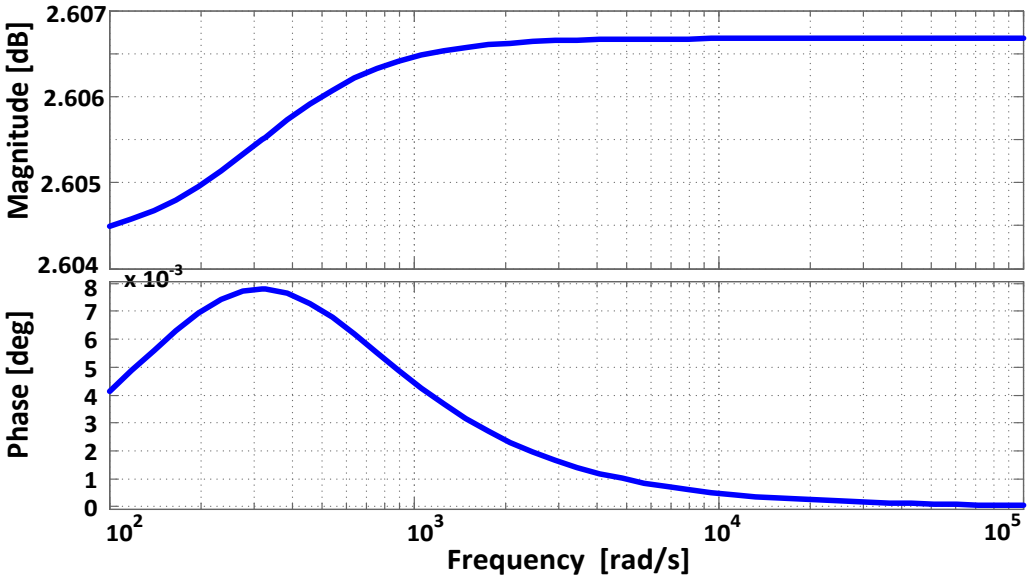

Fig. 6. Bode plot of the feeder with the DSTATCOM in open-loop mode.

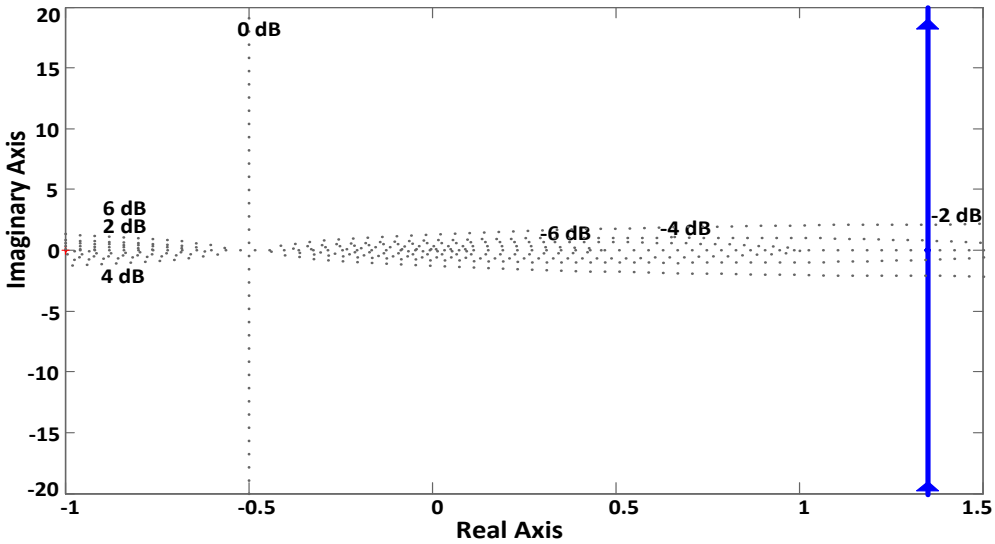

Fig. 7. Nyquist plot of the feeder with the DSTATCOM showing stability.

3.2. Simulation Results of the Feeder and the DSTATCOM

The designed feeder is implemented in MATLAB/Simulink under two conditions; light and heavy load. The light load was selected as $P = 10\%P_N = 0.45$ MW at p.f.= $\cos(\theta_N) = 0.8$ lagging. The heavy load was selected as $P = 100\%\ P_N = 4.5$ MW at p.f.= 0.8 lagging. These two cases were evaluated without/with DSTATCOM compensation.

3.2.1. Lightly Loaded Feeder

Figs. 8 and 9 show the lightly loaded feeder's line-to-line voltage waveforms at the receiving end without/with the DSTATOM compensation, respectively. Without the compensation (Fig. 8), the voltage increases drastically to 37.2 kV RMS, this is a *VR* of 14.24%. After compensation (Fig. 9), the voltage is maintained at 31.5 kV RMS but with distortion and $VR = 4.54\%$. The fast Fourier transform (FFT) analysis of the receiving end line voltage of this lightly loaded feeder is shown in Fig. 10 without the DSTATCOM for which the total harmonic distortion (THD) is 0.0%. The DSTATCOM succeeds in maintaining the voltage magnitude, but results a larger THD of 11.86% on the line voltage as shown in Fig. 11. The line currents without the DSTATCOM are shown in Fig. 12 with THD = 2.06% as shown on Fig. 13. When the DSTATCOM is applied, the line currents are shown by Fig. 14, with THD = 2.06% on Fig. 15.

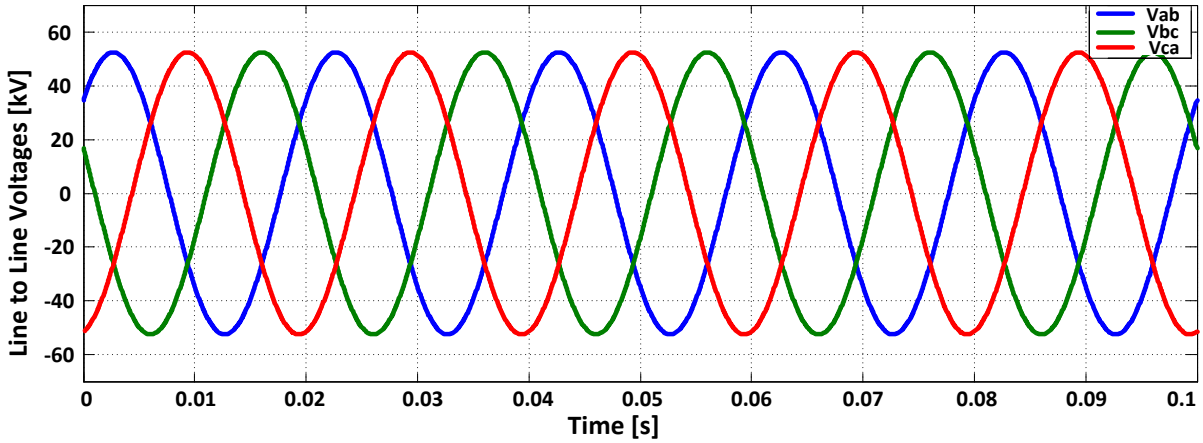

Fig. 8. The line-to-line voltage waveforms at the receiving end without DSTATCOM for light load.

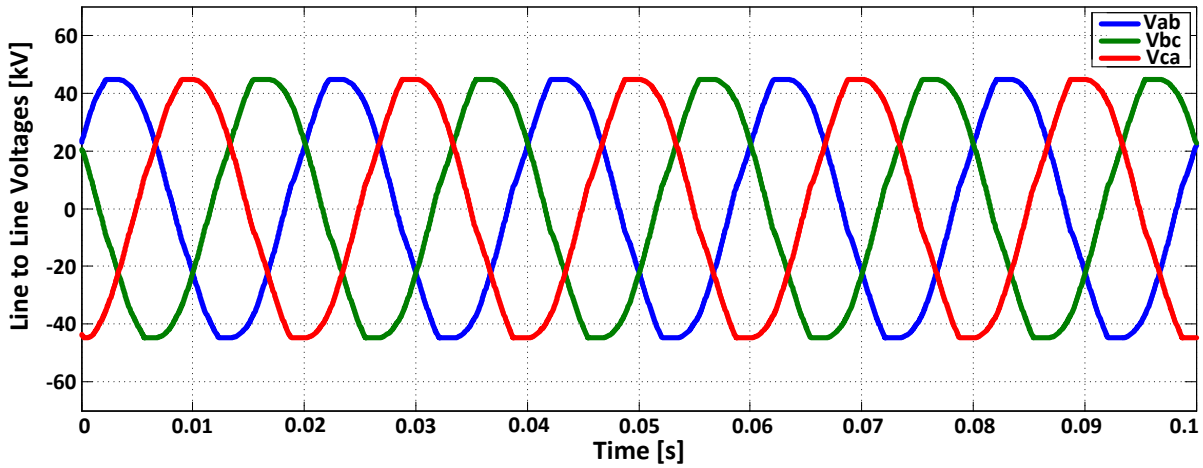

Fig. 9. The line-to-line voltage waveforms at the receiving end with DSTATCOM for light load.

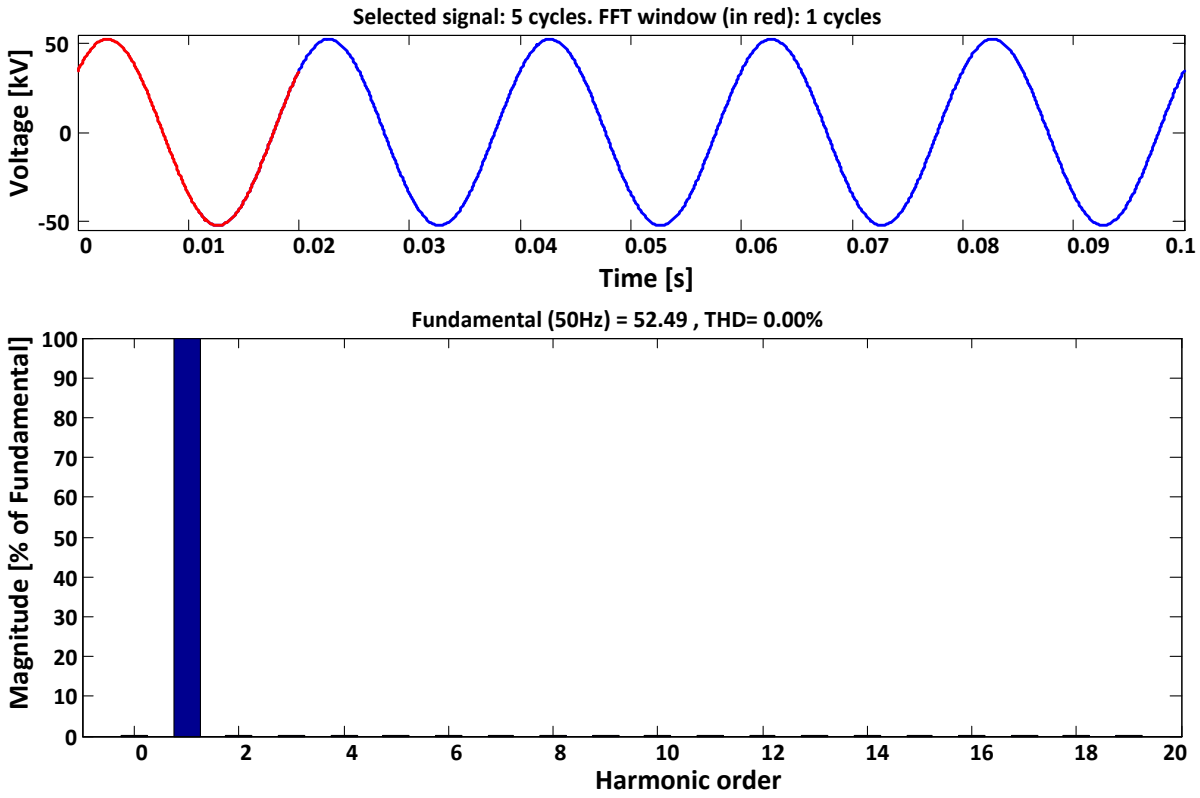

Fig. 10. The FFT of voltage waveforms at the receiving end without DSTATCOM for light load.

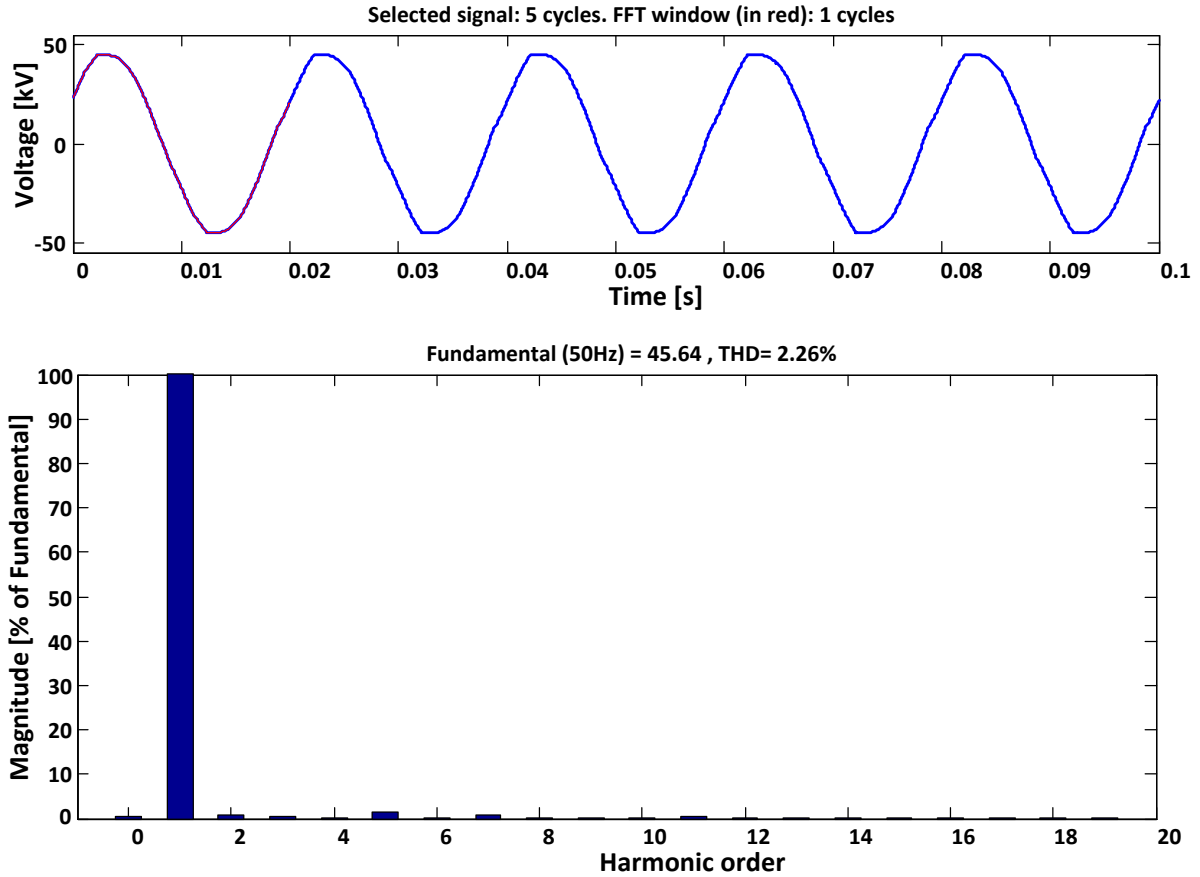

Fig. 11. The FFT of voltage waveforms at the receiving end with DSTATCOM for light load.

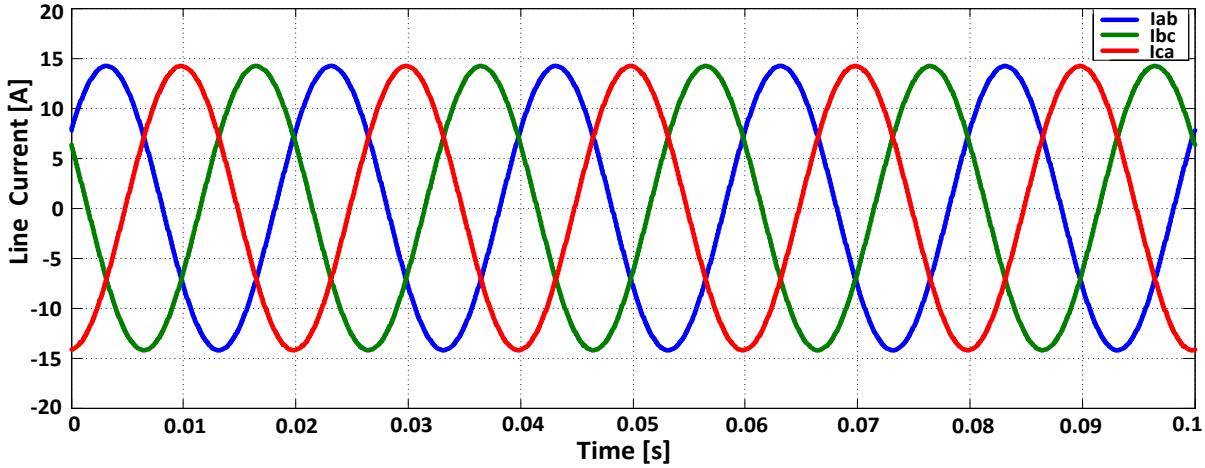

Fig. 12. The line current for light load without DSTATCOM.

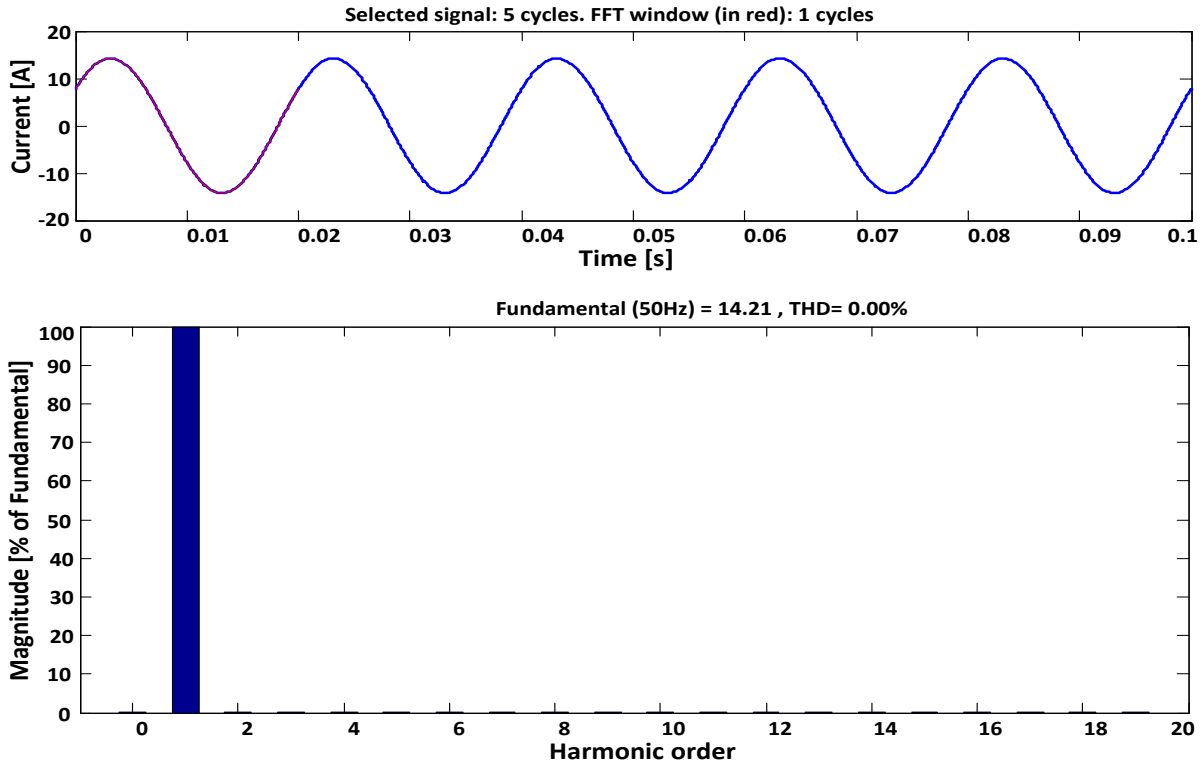

Fig. 13. The FFT of line current for light load without DSTATCOM.

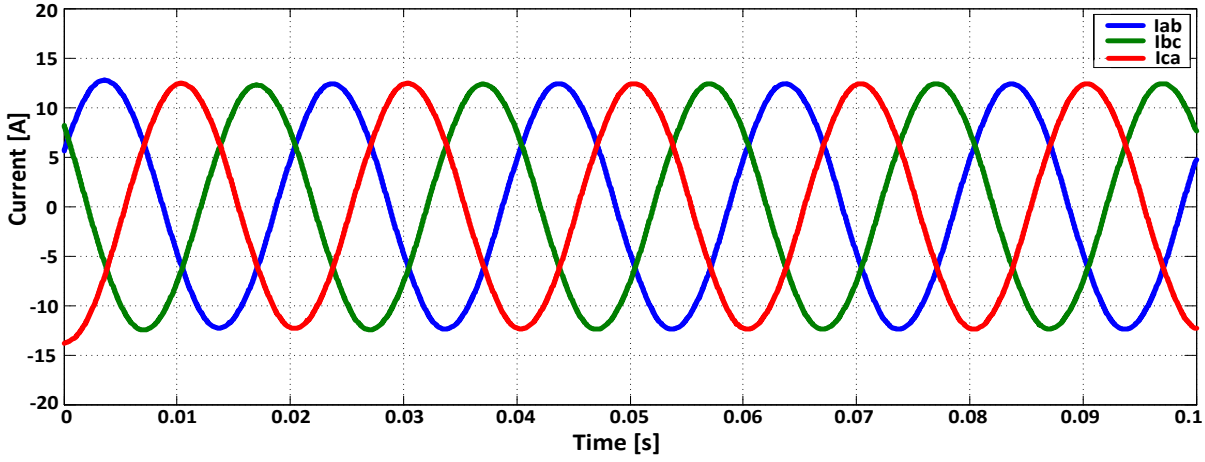

Fig. 14. The line current for light load with DSTATCOM.

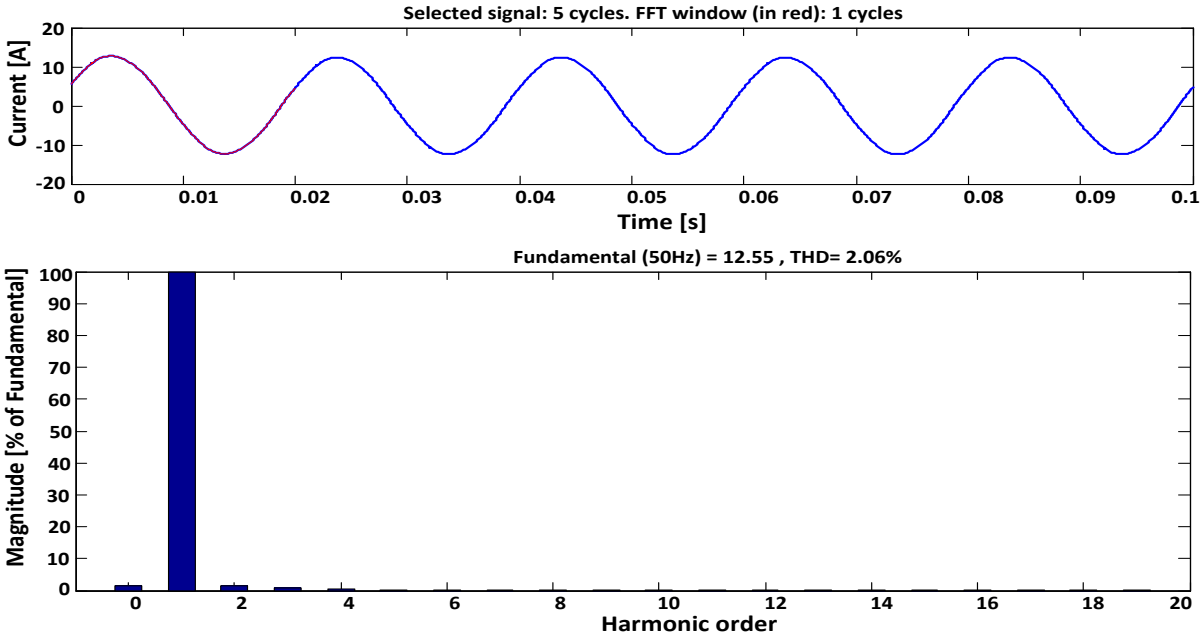

Fig. 15. The FFT of line current for light load with DSTATCOM.

3.2.2. Heavy Loaded Feeder

Figs. 16-23 show the heavy loaded feeder's line to line voltage waveforms at the receiving end without/with the DSTATOM compensation respectively. Without compensation (Fig. 16), the voltage drops to 28.45 kV RMS, this is a VR of 13.79%. After compensation, the voltage is maintained at 33.33 kV RMS (Fig. 17), a $VR = 1.01\%$; a very impressive improvement.

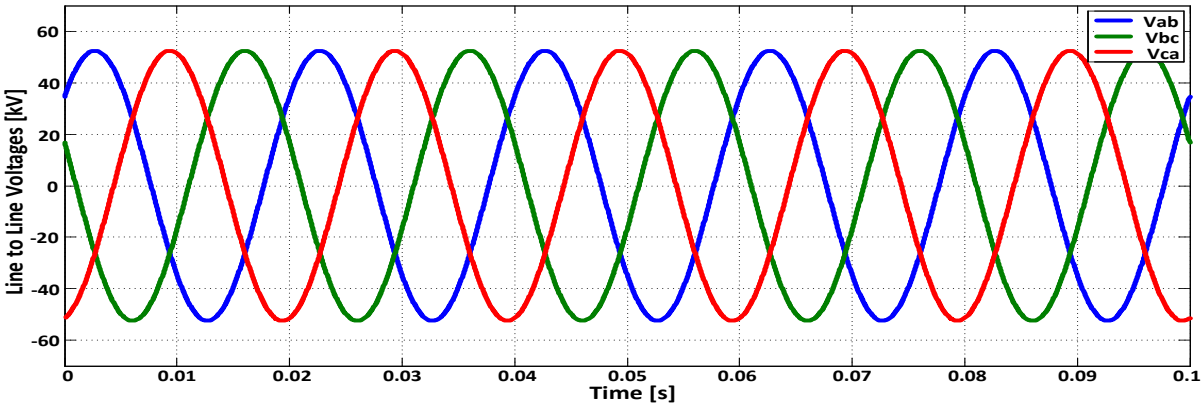

Fig. 16. The line-to-line voltage waveforms at the receiving end without DSTATCOM.

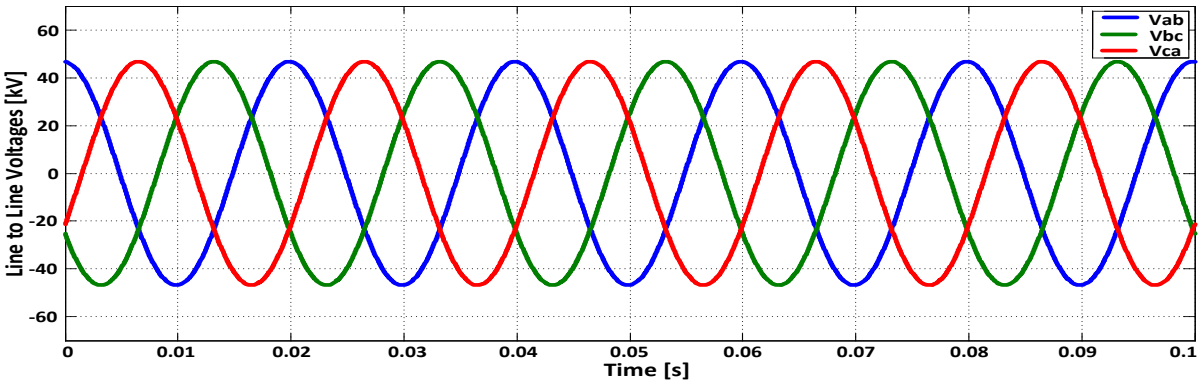

Fig. 17. The voltage waveforms for heavy load at the receiving end with DSTATCOM.

The FFT of the receiving end heavy load uncompensated feeder is displayed on Fig. 18, with THD = 0.0%. There is no distortion of the receiving end line voltage of the heavy load compensated feeder shown by FFT of Fig. 19 with THD = 0.0%. The line currents for the uncompensated heavy loaded feeder are shown by Fig. 20, with its FFT on Fig. 21 where THD = 0.0%. The line currents for the compensated heavy loaded feeder are shown by Fig. 22, with its FFT on Fig. 23 where THD = 0.0%.

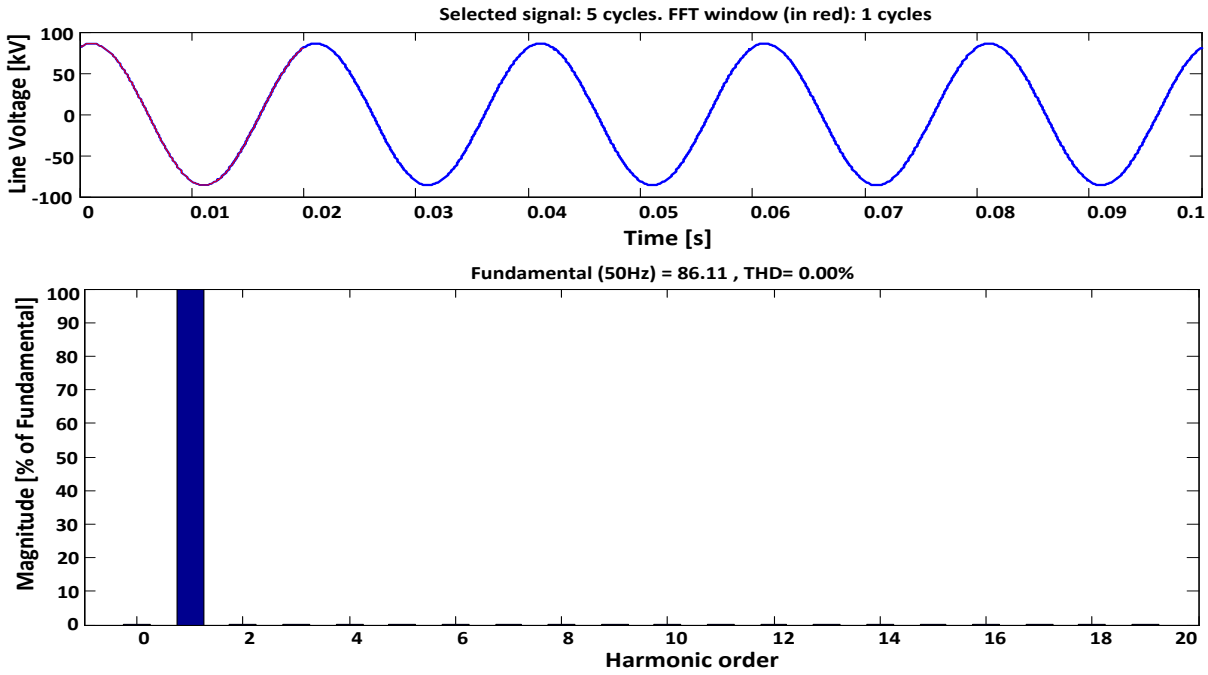

Fig. 18. The FFT of voltage waveforms at the receiving end without DSTATCOM.

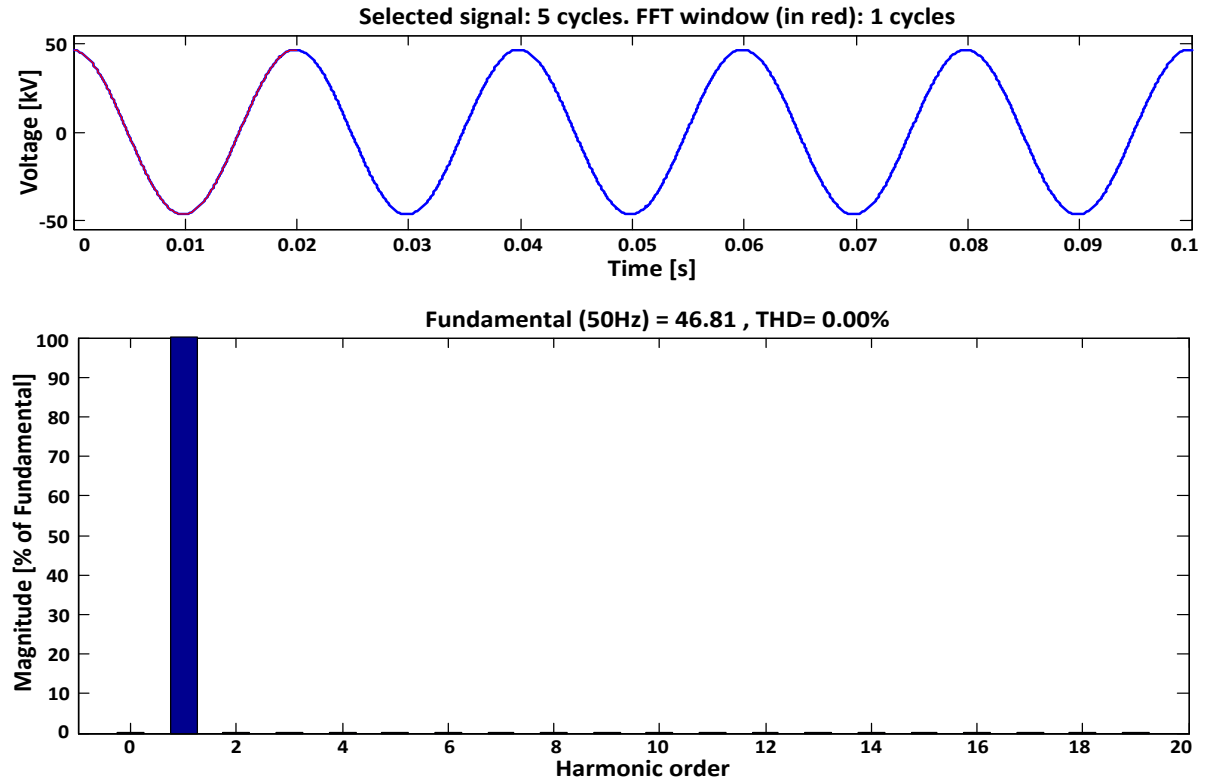

Fig. 19. The FFT of voltage waveforms at the receiving end for heavy load with DSTATCOM.

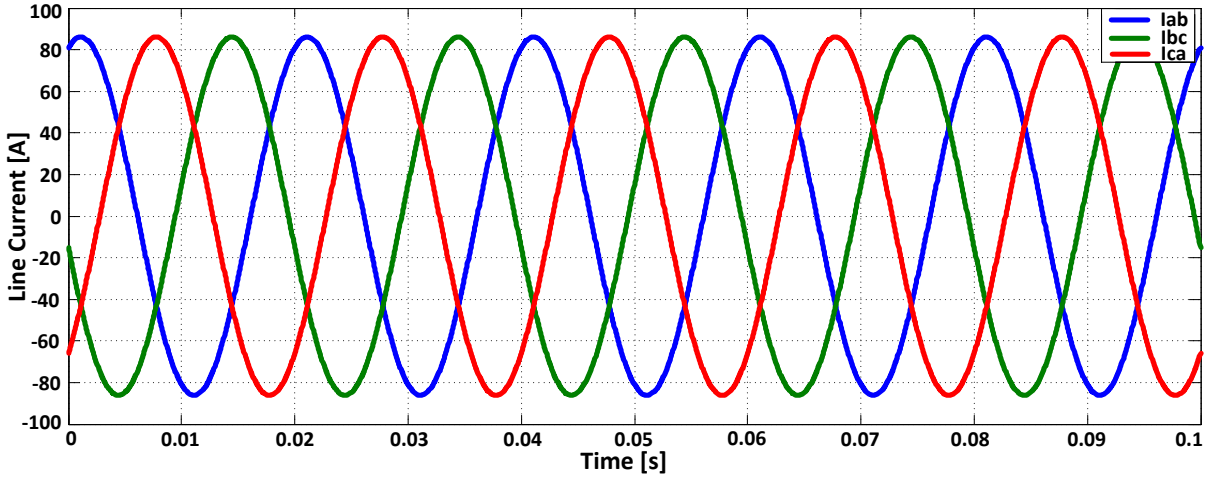

Fig. 20. Line current for heavy load without DSTATCOM.

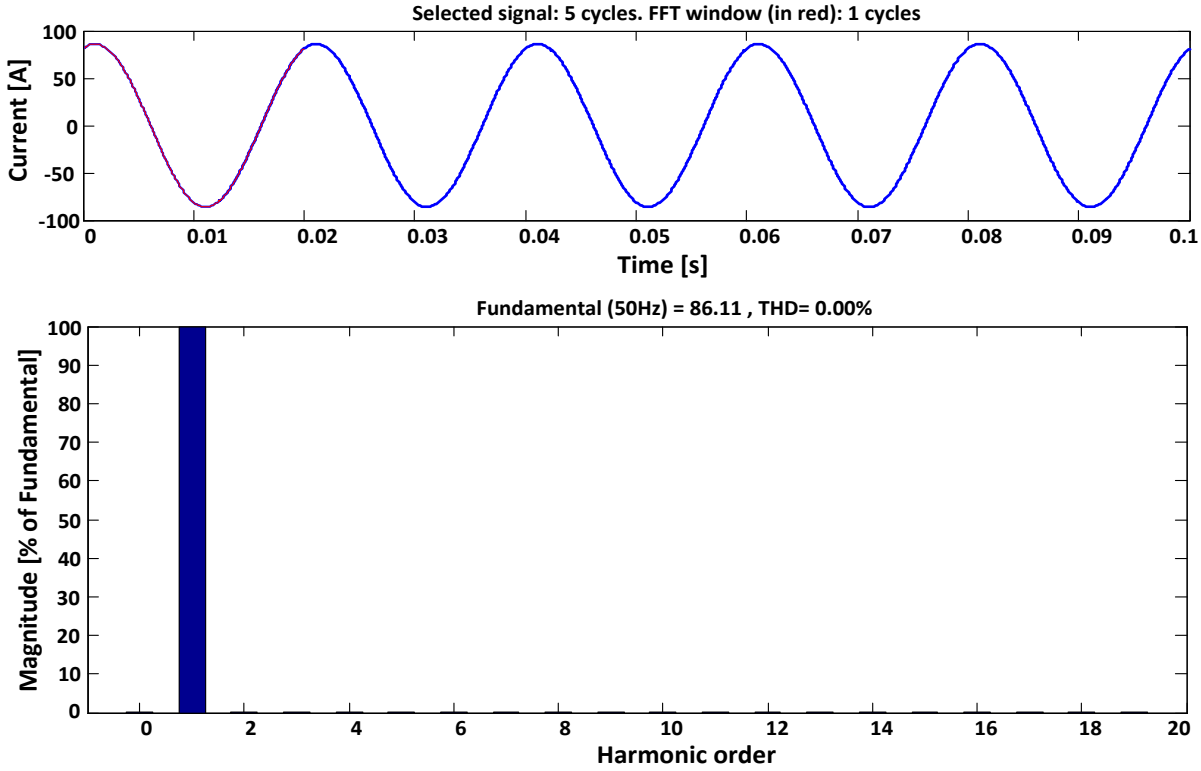

Fig. 21. The FFT of line current for heavy loaded feeder without DSTATCOM.

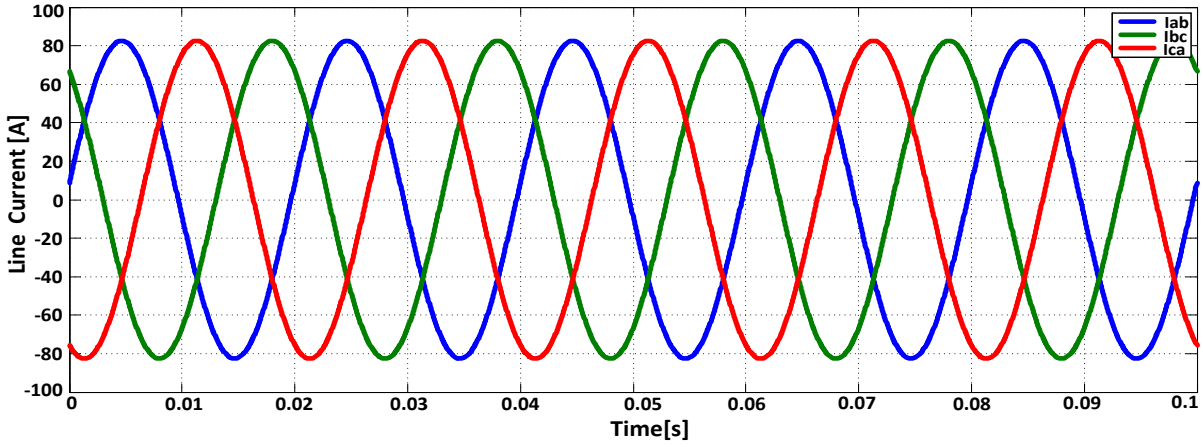

Fig. 22. Line current for heavy load with DSTATCOM.

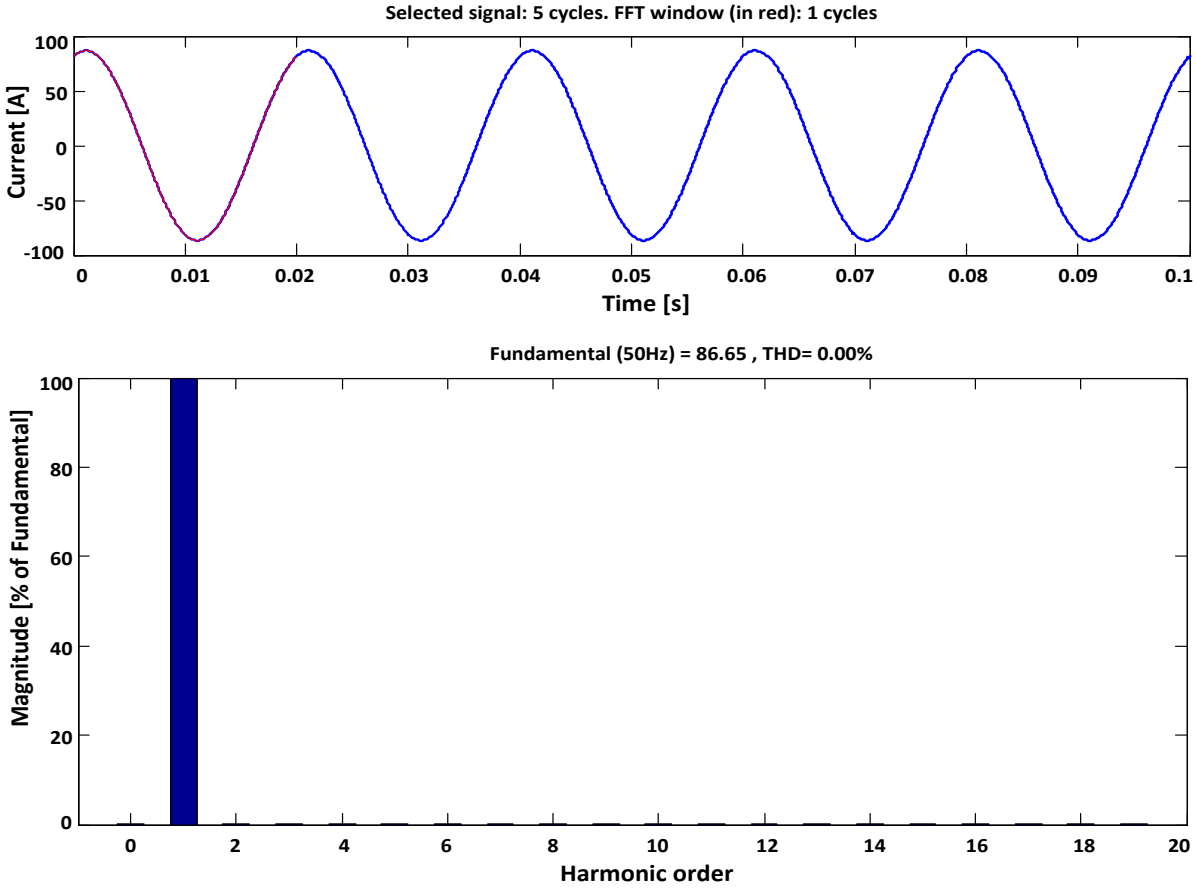

Fig. 23. The FFT of line current for heavy loaded feeder with DSTATCOM.

From these results it is seen that the DSTATCOM works as designed to keep the voltage of the light or heavily loaded feeder within acceptable limits in steady-state. By installing the DSTATCOM apart from controlling voltage, harmonics current can be reduced and frequency regulation can be achieved [14]. The DSTATCOM can improve power quality with the economical cost for power quality improvement [15]. The variation in voltage affects the power quality [16], and this paper has shown that the THD can be controlled using the proposed DSTATCOM for the Shinyanga-Bariadi feeder.

4. CONCLUSIONS

This paper has presented the design and performance evaluation of the 180 km, 33 kV RMS Shinyanga–Bariadi feeder. The feeder was modeled without DSTATCOM and also with DSTATCOM to evaluate the performance of the DSTATCOM. The DSTATCOM was modeled as a voltage source with reactance to improve the voltage profile at the receiving end during both light and heavy loading. Frequency analysis showed that the feeder with the DSTATCOM is stable in an open loop. Control algorithm based on PI was implemented on the DSTATCOM. Simulation results showed that the feeder with the DSTATCOM can keep the voltage at the receiving end within acceptable operating limits. Future work may focus on developing a dynamic model of the feeder with DSTATCOM so that transient analysis can be performed. Further, load flow studies considering the load demand of Maswa, Meatu, and Malampaka should be conducted to elucidate an improved voltage profile.

Acknowledgment: The authors would like to thank The University of Dar es Salaam for providing the space and environment to conceptualize the research, and Tanzania Electric Supply Company Ltd for giving access to the recorded data.

REFERENCES

[1] M. Irechukwu, A. Mushi, "Proposal for single-wire earth return distribution system for Homboza village electrification," *International Journal of Mechatronics, Electrical and Computer Technology*, vol. 11, no. 39, pp. 4837–4842, 2021.

[2] G. Mhagama, *Determination of DSTATCOM Parameters for a* 33 *kV Line From Shinyanga To Bariadi*, M.Sc. Thesis, Dar es Salaam: University of Dar es Salaam, 2017.

[3] L. Gyugi, "Power electronics in electric utilities: static VAR compensators," *Proceedings of the IEEE*, vol. 76, no. 4, pp. 483–494, 1988.

[4] H. Zhao, L. Li, X. Zeng, "General mixed norm-based adaptive control algorithm for distribution static compensator," *IFAC papers online*, vol. 52, no. 24, pp. 168-173, 2019.

[5] A. Rohani, M. Joorabian, M. Abasi, M. Zand, "Three phase-amplitude adaptive notch filter control design of DSTATCOM under unbalanced/distorted utility voltage conditions," *Journal of intelligent and fuzzy systems*, vol. 37, pp. 847-865, 2019.

[6] Tanzania Electric Supply Company, *Shinyanga Substation Logbook Report*, 2016.

[7] IEC 60287-1-1, *Electric Cables – Calculation of Current Rating – Part 1: Current Rating Equations (100% Load Factor) and Calculation of Losses – Section 1: General*, 2006.

[8] J. Riba, "Analysis of formulas to calculate the AC resistance of different conductors' configurations," *Electric Power Systems Research*, vol. 127, pp. 93-100, 2015.

[9] M. El-Hawary, *Electrical Energy Systems*, Boca Raton: CRC Press, 2000.

[10] J. Grainger, W. Stevenson, *Power System Analysis*, New York: McGraw Hill, 1994.

[11] J. Guerrero, P. Loh, T. Lee, M. Chandorka, "Advanced control structures for intelligent microgrids-part II: power quality, energy storage, and AC/DC microgrids," *IEEE Transactions on Industrial Electronics*, vol. 60, no. 4, pp. 1263-1269, 2013.

[12] K. Kerrouche, E. Lodhi, M. Kerrouche, L. Wang, F. Zhu, G. Xiong, "Modeling and design of the improved D-STATCOM control for the power distribution grid," *SN Applied Sciences*, vol. 2, no. 1519, pp. 1-11, 2020.

[13] P. Roncero-Sanchez, E. Acha, "Design of a control scheme for distribution static synchronous compensators with power-quality improvement capability," *Energies*, vol. 7, pp. 2476-2497, 2014.

[14] O. Mahela, A. Shaik, "Power quality improvement in distribution network using DSTATCOM with battery energy storage system," *Electrical Power and Energy Systems*, vol. 83, pp. 229-240, 2016.

[15] M. Mangaraj, A. Panda, "Performance analysis of DSTATCOM employing various control algorithms," *IET Generation, Transmission and Distribution*, vol. 11, no. 10, pp. 2643-2653, 2017.

[16] J. Hussain, M. Hussain, S. Raza, M. Siddique, "Power quality improvement of grid-connected wind energy system using DSTATCOM-BESS," *International Journal of Renewable Energy Research*, vol. 9, no. 3, pp. 1388-1397, 2019.